A Receiver Architecture for Pulse-based Electromagnetic Nanonetworks in the Terahertz Band

Raul Gomez Cid-Fuentes[*], **Josep Miquel Jornet**[*], **Ian F. Akyildiz**[*†] and **Eduard Alarcón**[†]

[*] Broadband Wireless Networking Laboratory
School of Electrical and Computer Engineering, Georgia Institute of Technology, Atlanta, Georgia 30332, USA
Email: {raul.gomez, jmjornet, ian}@ece.gatech.edu

[†] NaNoNetworking Center in Catalunya (N3Cat)
Universitat Politècnica de Catalunya, 08034 Barcelona, Spain
Email: ian@ac.upc.edu, eduard.alarcon@upc.edu

Abstract—Graphene-enabled wireless communications set the Terahertz Band as the frequency band of operation of future nanodevices (0.1-10 THz). Amongst others, femtosecond-long pulse-based modulation schemes have been recently proposed to enable the communication among nanodevices. Within this context, a receiver architecture suitable for nanodevices must be ultra compact, must have high sensitivity and must be ultra-low power. Unfortunately, common receiver architectures used in other communication schemes, such as IR-UWB, show a strong compromise between low complexity and performance. In this paper, a novel receiver architecture for pulse-based communication based on a Continuous-time Moving Average (CTMA) symbol detection scheme is presented. This scheme bases its symbol decision on the received signal power maximum peak after the CTMA, which is implemented with a single low-pass filter. Moreover, an analytical model for the symbol detection is provided and it is quantitatively shown that the proposed CTMA scheme outperforms previous symbol detection schemes for pulse-based modulations in terms of Symbol Error Rate (SER). The low complexity and relaxed synchronization needed for this symbol detector makes this structure specially suited for the development of future transceivers for nano-devices.

Fig. 1.   Receiver Block diagram Architecture.

I. INTRODUCTION

Nanotechnology is enabling the development of devices in a scale between one and a few hundred nanometers. One of the early applications of these nano-devices is in the field of nanosensing. For example, nanosensors can detect extremely low concentrations of chemical compounds with unprecedented accuracy [1]. The applications of nanosensors can be found in very diverse fields ranging from advanced health monitoring systems [2] to air pollution control [3].

For the time being, the tasks that individual nanodevices can accomplish are very limited in terms of complexity. Communication among nanodevices will expand the applications and capabilities of a single nanodevice through collaborative effort. This paradigm can provide high complexity applications in a distributed manner over larger areas [4].

Novel nanomaterials such as graphene are enabling the development of miniaturized electromagnetic (EM) transceivers [5], [6]. Graphene-based radio-frequency (RF) nano-components [7] and graphene-based nano-antennas [8] set the Terahertz Band (0.1-10.0 THz) as the expected frequency range of operation for the future EM nano-transceivers.

As we showed in [9], the Terahertz Band provides a huge bandwidth in the short range that can support very high transmission rates, up to hundreds of terabits per second. However, this may not always be required
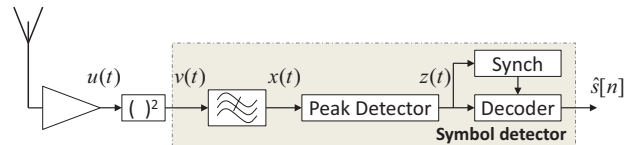
Consistently with the trends of ultra-low power, compact-size and ultra-low complexity design in broadband communications, such as IR-UWB [10], pulse-based communication has been recently proposed for nanodevices. As an example, the Time-Spread On-Off Keying (TS-OOK) has been proposed in [11]. This scheme is based on the asynchronous exchange of femtosecond-long pulses following an On-Off modulation spread in time, to exploit the Terahertz channel behavior.

In this context, we present a new receiver architecture for pulse-based communications based on a Continuous-time Moving Average (CTMA) symbol detection scheme. This scheme bases its decision in the received signal power maximum peak after the CTMA, which is implemented with a single low-pass filter. Afterwards, to decode the symbol, this maximum is compared with a previously defined threshold. This scheme outperforms, in terms of simplicity and robustness, existing receiver architectures [12], [13], [14], which are mainly based on an *integration and sampling* approach.

The main contributions of this paper can be summarized as follows:

- We propose a novel receiver architecture for EM nanonetworks based on a CTMA symbol detection scheme.
- We develop an analytical model for the symbol detection probability and investigate the impact of different system parameters of the receiver architecture on the Symbol Error Rate (SER).
- We develop a regression model to simplify the estimation of the symbol receiver SER and we explore the impact that the intersymbol interference (ISI) has over the maximum achievable bitrate.

The rest of this paper is organized as follows. In Sec. II we describe the symbol detection mechanism in the proposed receiver architecture. In Sec. III, we develop an analytical model to estimate its SER. In Sec. IV we validate the model and evaluate the performance of the receiver. In Sec. V we conclude our work.

II. Symbol Detection

The symbol detector presented in this paper consists of a low pass filter which approximates a CTMA, a peak detector, a decision maker implemented in the decoder and the sampling provided by the synchronization block. The symbol detection block diagram is shown in Fig. 1 within a suggested receiver architecture based on power detection. As shown, the symbol detector is located after a Terahertz front-end, which amplifies and conditions the input signal, and a power detector. The power detection has been well explored in other non-coherent pulse-based communication schemes, and it is shown that it can achieve up to 10 times power consumption savings [15].

Usual symbol detectors sample the output of a switched integrator in a single instant of time. In particular, in optical schemes [16], the symbol reception is phase-synchronized using Phase Locked Loop (PLL), so the output can be sampled at the optimal point. In carrier-less communications, such as IR-UWB [12], phase synchronization is highly discouraged, so the received signal power is integrated over a time window wider than the pulse time. Afterwards, the output value is sampled at the end of the integration time. Both cases need high synchronization between devices before the transmission starts. To relax the synchronization constraints in the expected time interval of arrival in IR-UWB, the integration time window is increased in the order of 10 to 100 times the pulse time T_p, so the pulse can fit into the integration window [13]. This significantly lowers the performance of the receiver due to the fact that the *useful* signal power is averaged with respect to the extra noise power (See Fig. 2.a).

A. Continuous-time Moving Average

As shown in Fig. 2.a, when the receiver integrates the pulse over a time window which is greater than the pulse time, the noise contribution proportionally increases with this time window. This effect drops the performance of the receiver in terms of SER by reducing the signal-to-noise ratio. There is a compromise between simplicity and minimum energy per bit.

To mitigate this noise effect, we need to reduce the integration time up to the pulse time length, T_p. However, since the expected time interval, T, is still kept in the order of 10 to 100 times the pulse time, we need to implement a total of T/T_p integrators in parallel and decide after the pulse reception which one has integrated the pulse energy. This makes this implementation impractical for low complexity devices.

As shown in Fig. 2.b, there is a probability that the pulse does not perfectly fit in the integration time window. To make this happen we either must delay the integrators by a $\Delta\tau$ time (see Fig. 2.c) or we must increase the number of integrators. By overlapping them we make sure that the pulse can fit in one of them. However, by increasing the number of integrators, the receiver complexity is also increased.

Since we can consider that, due to the asynchronous nature of pulse-based communication, the delay $\Delta\tau$ is unknown, we need overlap infinite T_p time windows delayed a $\Delta\tau$ tending to zero. Under this assumptions, we define the Continuous-Time Moving Average (CTMA) as the linear time-invariant (LTI) system with input to output relation defined as:

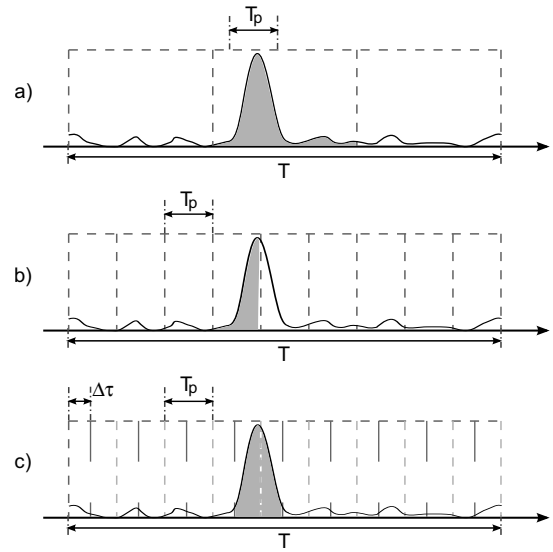$$x_{CTMA}(t) = \int_{t-T_p}^{t} v(t)dt \qquad (1)$$

Fig. 2. CTMA symbol detection. a) The integration time window is greater than the pulse time so additional noise is also integrated. b) The integration time window is reduced to the pulse time, the pulse does not fit into the time window. c) Thanks to CTMA, there are infinite T_p integration time windows over the time T so the pulse fits into only one of these time windows.

where T_p is the pulse time, $v(t)$ refers to the input of the LTI system and x_{CTMA} stands for its output.

This LTI system implements for each time t_i the integration over a pulse time T_p of the input power during the time interval $(t_i - T_p, t_i)$. Thus, this LTI system implements the infinite number of integrators needed to fit the upcoming pulse into one of the integrators over T. We refer as t_j the time that makes the upcoming pulse to perfectly fit into the integration window and $x(t_j)$ the result of this integration.

However, the limited time resolution is fixed to the whole expected time interval T, so the possibility of trying to detect the time t_j and its value $x(t_j)$ is discarded. Notice that, in a noise-free situation, the maximum value of the signal $x(t)$ is given when the pulse perfectly fits into the time window, thus we have that $\max x(t) = x(t_j)$ while when silence is transmitted, the maximum is still kept as zero. Thus, we use the $\max x(t)$, which provides a good estimator of $x(t_j)$, to decode the received symbol.

An ideal CTMA symbol detection scheme is not implementable. We next describe how we approximate this system using a low pass filter and how we detect the pulses to keep simple the symbol detector, so we can guarantee the future integration of this symbol detector into simple nanodevices.

B. Low-Pass Filter-based CTMA

Lumped elements are usually proposed to approximate rectangular impulse responses by means of reactance networks [17]. Due to simplicity constraints, we approximate this CTMA using a second order low-pass filter. This filter could be easily implemented with a chain of two RC filters in cascade with orders of magnitude of R $\sim$ kΩ and C $\sim$ fF, or even solutions implemented with graphene transistors, since their model implicitly provides a low-pass behavior [18].

To determine the cutoff frequency or, equivalently, the time width of the low-pass filter, we propose a square error minimization between both impulse responses as a function of the a parameter, defined in the low-pass filter impulse response

$h_{lpf}(t)$, and the pulse time T_p, defined in the impulse response $h_{CTMA}(t)$ of the CTMA. These impulse responses are given by:

$$h_{CTMA}(t) = \begin{cases} \frac{1}{T_p} & \text{If } 0 < t < T_p \\ 0 & \text{Otherwise} \end{cases}, \quad h_{lpf}(t) = a^2 t e^{-at} \quad (2)$$

where h_{CTMA} is the impulse response of an ideal integrator with T_p time of integration and h_{lpf} refers to the impulse response of a second order low-pass filter with two real poles with parameter a. In order to find the closer low-pass filter to the ideal integrator, we have minimized the square error between both impulse responses as function of the parameter a. This minimization is given for $a = 1.4615/T_p$.

C. Peak Detection and Decoding

To accordingly decode the symbol received, we introduce a peak detector and a decoder. These two blocks, which are aided by the synchronization block, decode the symbol according to:

$$\hat{s}[n] = \begin{cases} 1 & \text{if } \max_{t \in (0,T)} x(t) > V_{th} \\ 0 & \text{otherwise} \end{cases} \quad (3)$$

The proposed peak detector is based in a continuous-time comparison. This is integrated by a comparator and a latch circuit that, whenever the input is higher than the predefined threshold, the output of the circuit is fixed to "1" until an external control circuit resets the output to "0". This comparator starts operating anytime the expected time interval starts. This timing is provided by the synchronization block.

Once the expected time interval has reached the end, the decoder aided by the synchronization block checks the output of the peak detector and decodes the symbol. Additionally, since the symbol detector is not integrating the signal during all the expected time interval T, but only during a time T_p, the decoder can oversample its input a few times over the expected time interval to decide whether the pulse has already arrived. This possibility can open up very interesting but simple symbol time estimation schemes for symbol detection.

Notice that, although no maximum function is carried out in the real reception, if at a time t_j, $x(t_j)$ is above the threshold, the maximum value $x(t_i)$ must be also above this threshold. However, the consideration of the maximum value is encouraged to model the symbol detector performance.

III. ANALYTICAL MODEL FOR THE SYMBOL DETECTION

The output of the Low-pass filter, $x(t)$, can be written for a single pulse arriving at a random time τ as:

$$x(t) = \left(s[i]w(t - iT_s - \tau) * h_c(t) + n(t) \right)^2 * h_{lpf}(t) \quad (4)$$

where $*$ denotes convolution, $s[i]$ stands for the transmitted symbol which can be either "0" or "1", $w(t)$ refers to the 100 femtosecond-long pulse, T_s is the symbol period, $h_c(t)$ stands for the transfer function provided by the channel, $n(t)$ refers to the noise of bandwidth W and $h_{lpf}(t)$ is the impulse response of the low-pass filter.

Then $\hat{s}$ is decoded according to (3). To model $\max x(t)$, we consider that the SER tends to the ideal energy detector receiver when the time of observation tends to zero. The low-pass filter provides a high correlation between consecutive instants of time that enables the discretization of the continuous-time function $x(t)$ into N independent random variables.

Then, $\max x(t)$ can be expressed as function of the vector $\boldsymbol{X} = \{X_1, X_2, \cdots, X_N\}$ which refers to the discretized function $x(t)$ with:

$$\max_{t \in (0,T)} x(t) = \max_N \boldsymbol{X} = \max_N \{x(t_1), x(t_2), \cdots, x(t_N)\} \quad (5)$$

where T refers to the time of observation, N stands for the number of independent discretized variables, and $x(t_1), \cdots, x(t_N)$ is the value of the input signal $x(t)$ at the $t_1, \cdots, t_N$ instants.

A. Detection of Logical "0"

In pulse-based On-Off keying modulation schemes, such as TS-OOK, a logical "0" is transmitted as silence [11]. When silence is transmitted, just noise is detected in the receiver, so there is no reason why the components of $\boldsymbol{X}$ might be different. For this we can consider $\boldsymbol{X}$ as a vector with identically N random variables, with probability density function $f_n(y)$. The probability density function of $\max \boldsymbol{X}$ can be expressed as a function of $f_n(y)$ by:

$$f_{max,n}(y, N) = N F_n(y)^{N-1} f_n(y) \quad (6)$$

where N is the number of discrete random variables, $f_n(y)$ refers to the probability density function of a single x_i variable and $F_n(y)$ stands for its cumulative distribution function. Each X_i corresponds to the square value of the noise signal over the bandwidth provided by the low-pass filter. This is commonly modeled in the literature as a chi-square distribution with $v = 2T_pW$ degrees of freedom random variable [19], with T_p the pulse time and W its bandwidth. This probability density function is expressed in terms of the normalized random variable $Y = 2X/N_{00}$, for a two sided power spectral noise density $N_{00}/2$ and is given by:

$$f_n(y) = \frac{1}{2^{v/2}\Gamma(\frac{v}{2})} y^{(v-2)/2} e^{-y/2}, \quad y \geq 0 \quad (7)$$

where Γ is the gamma function, v refers the degrees of freedom and y the normalized random variable.

In particular, if TS-OOK and ultra-short pulse modulations uses $T_pW = 1$, we obtain for $f_{max,n}(y, N)$:

$$f_{max,n}(y, N) = \frac{1}{2} N \left(1 - e^{-y/2}\right)^{N-1} e^{-y/2}. \quad (8)$$

however, only if the pulse is strictly 100 fs long, this condition is valid. Since the n-th time derivative of a Gaussian pulse is considered for the pulse generation, and also the low-pass filter is an approximation of an ideal integrator, values of T_pW are expected to be higher. In particular, for a second time derivative Gaussian pulse we have $T_pW = 3.5$. For this, there is no closed-form expression of $f_{max,n}(y, N)$ so that the function must be numerically evaluated.

B. Detection of Logical "1"

A logical "1" is transmitted by using a femtosecond-long pulse [11]. The signal x(t) received is noise plus signal during a very short time and noise during most of the time. This fact leads to consider two different types of random variables,

namely N_n independent noise random variables with $f_n(y)$ distribution and N_s random variables with $f_{sn}(y)$ distribution. Then, in this case we can express the maximum as:

$$\max_N \boldsymbol{X}_{sn} = \max_N \{\boldsymbol{X}_{n,N_n}, \boldsymbol{X}_{s,N_S}\} \qquad (9)$$

where $\boldsymbol{X}_{sn}$ refers to the vector containing the random variables that model a pulse in reception, $\boldsymbol{X}_{s,N_s}$ stands for the vector of N_s random variables that model $x(t)$ when a pulse is being received. $\boldsymbol{X}_{n,N_n}$ is the vector containing noise with N_n identically distributed independent random variables. The total number of random variables of noise and signal must be kept equal to $N = N_n + N_s$ since N is function of the time interval. Then, its probability density function can be written as:

$$f_{max,sn}(y, N_s, N_n) = F_{max,s}(y, N_s) f_{max,n}(y, N_n) \\ + f_{max,s}(y, N_s) F_{max,n}(y, N_n) \qquad (10)$$

where $f_{max,sn}(y, N_s, N_n)$ is the probability density function of $\max x(t)$ when transmitting a pulse in terms of the normalized random variable $Y = 2X/N_{01}$, with N_s and N_n random variables, $f_{max,s}(y, N_s)$ stands for the probability density function of the maximum of $\boldsymbol{X}_{s,N_s}$, with $F_{max,s}(y)$ its cumulative distribution function, $f_{max,n}(y, N_n)$ the probability density function of $\max \boldsymbol{X}_{n,N_n}$ and $F_{max,n}(y, N_n)$ its cumulative distribution function. Each component of $\boldsymbol{X}_{s,N_s}$ is characterized by the probability density function $f_s(y)$. Similar to $f_n(y)$, $f_s(y)$ is usually modeled in the literature as a normalized non-central chi-squared distribution with $v = 2T_pW$ degrees of freedom with the normalized random variable $Y = 2X/N_{01}$ for a two sided power spectral noise density $N_{01}/2$ [19]. This is given by:

$$f_s(y) = \frac{1}{2}\left(\frac{y}{\lambda}\right)^{(v-2)/4} e^{-(y+\lambda)/2} I_{(v-2)/2}(\sqrt{(y\lambda)}) \qquad (11)$$

where $\lambda = 2E/N_{01}$ refers to the non-centrality parameter and $I_n(z)$ stands for the nth order modified Bessel Function of the first kind. $f_{max,s}(y)$ can be expressed by using(6).

However, provided that the noise level must be kept lower than the signal level to guarantee a certain SER, $\max_N \boldsymbol{X}_{sn} = \max_N \{\boldsymbol{X}_{n,N_n}, \boldsymbol{X}_s\} \approx \max_{N_s} \{\boldsymbol{X}_s\}$, and then:

$$f_{max,sn}(y, N_s) = f_{max,s}(y, N_s). \qquad (12)$$

In any case, since $f_{max,s}(y, N_s)$ is not solvable, $f_{max,sn}(y, N_s, N_n)$ cannot lead to a closed-form expression.

C. Threshold and SER

The performance of the symbol detector can be expressed in terms of the error detection probability of every symbol, and averaging them by their symbol probability. The error detection probabilities for both symbols are defined as:

$$P_{\epsilon|s=0} = \int_{2V_T/N_{00}}^{\infty} f_{max,n}(y, N) dy , \\ P_{\epsilon|s=1} = \int_{0}^{2V_T/N_{01}} f_{max,sn}(y, N) dy \qquad (13)$$

where V_T stands for the threshold, N_{00} and N_{01} refer to the noise level for the symbols "0" and "1" respectively and $f_{max,n}(y, N)$ and $f_{max,sn}(y, N)$ are the probability density functions for the symbols "0" and "1".
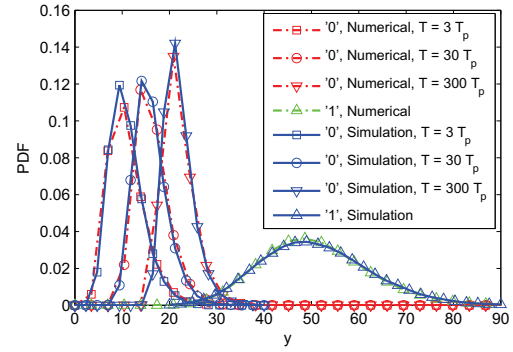

Fig. 3. Probability density function of $\max x(t)$ when receiving logical "0"s and "1"s for a distance of 66 mm in the Terahertz channel.

Finally, we seek to obtain the probability of symbol error. This SER varies as function of the detection threshold and can be expressed as:

$$SER = P_{\epsilon|s=0}\, p_{s=0} + P_{\epsilon|s=1}\, p_{s=1} \qquad (14)$$

where $P_{\epsilon|s=0}$ and $P_{\epsilon|s=1}$ refers to the detection probabilities in (13) and $p_{s=0}$ and $p_{s=1}$ the symbol probability. This optimization is not analytically solvable so in the following section, this is numerically evaluated.

IV. PERFORMANCE EVALUATION

In this section, we validate the expressions for the probability density functions of both symbols, "0" and "1", throughout simulation. We analyze the performance of the receiver and the symbol detector in terms of SER as a function of the channel attenuation and noise.

A. System Model

The following assumptions are considered in our analysis:

- The path-loss and noise in the Terahertz Band are computed by using the models introduced in [9]. A standard medium with 10% of water vapor is considered.
- Although the channel is asymmetric [9], we suppose the worst case scenario where the noise level for both symbols is considered the same, and we refer this noise level as $N_0 = N_{00} = N_{01}$. This is due to the fact that a pulse from another transmitting nanodevice can excite the channel just before the symbol "0" is transmitted.
- Only the channel noise has been taken into account in the numerical and simulation results, since no specific technology has been considered to implement the transceiver and, thus, a receiver noise model is not available.
- The transmitter encodes logical "1"s by using 100 femtosecond-long Gaussian pulses with an energy equal to 1 picoJoule. The second time-derivative of the Gaussian pulse is supposed to be detected in the receiver. The logical "0" is transmitted as silence.
- The symbol probabilities are considered equal for the logical "1"s and "0"s. $p_{s=0} = p_{s=1} = 0.5$.

B. Model Validation

In order to validate the symbol detection probability model, we compare the numerical results of the analytical model given by (8) and (11) with the simulation results given by the emulation of the receiver block diagram from Fig. 1 when receiving the symbols "0" and "1". In this simulation, the
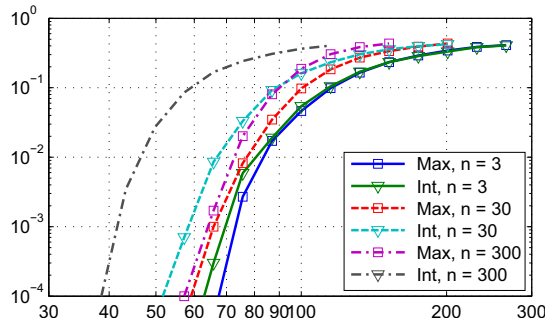
Fig. 4. Comparison between the SER provided by the proposed receiver and the state-of-the-art receiver architecture for different time intervals in the Terahertz channel.

Fig. 5. Comparison between the SER provided by the proposed receiver and current receiver in terms of $n = T/T_p$.

second time-derivative of a 100 femtosecond-long Gaussian pulse has been implemented. The values of the energy per bit and the noise level chosen belong to a distance between devices of 66 mm. Using this pulse, the pulse time-bandwidth product is $T_p W = 3.5$. The normalized results of the simulations are shown superimposed over the numerical results in Fig. 3. The simulation results provide the random variable $\max x(t)$. To match results, we have appropriately normalized this variable to $Y = 2X/N_{00}$ when a logical "0" is received or to $Y = 2X/N_{01}$ when the pulse received is a logical "1".

1) Logical "0": In Fig. 3, the probability density function for the detection of a logical "0" is represented for three different time intervals $T = \{3, 30, 300\}$ T_p. These three time intervals can be discretized by a number $N = \{2, 15, 110\}$ of random variables. As shown, the average value presents logarithmic growth with this time interval.

2) Logical "1": The probability density function for the detection of this symbol is represented. The time for the detection of this symbol can be discretized by a number $N_s = 2$ of random signal variables. The fact that this probability density function does not present any variation with the time interval length validates the approximation proposed in (12). To observe the effect of the time interval in the variation of the logical "1" requires very large time intervals or very low E/N_0 ratio, which leads to very bad values of SER. This last particular case is out of our study because a SER in the order of 10^{-3} to 10^{-4} is the usual target in communications.

C. SER Estimation

Fig. 4 shows the SER estimation as a function of the distance. In the figure, three curves, referred as *Max*, show the proposed architecture estimated SER for the values of $n = T/T_p = \{3, 30, 300\}$. Equivalently, three curves for the same values of n are shown for classic receiver architectures based on integration over the time interval T. These curves are referred as *Int*. As the figure shows, decreasing the integration time to T_p by using the CTMA mitigates the impact of noise. This makes the proposed receiver to outperform the existing receivers by increasing up to a 50% the maximum distance for a relation $n = T/T_p = 300$, in order to guarantee a SER of 10^{-4}.

Moreover, from the figure, we observe the strong impact that the molecular absorption has over the attenuation and noise in terms of the distance. A distance increase of around a 10% drops the SER in several orders of magnitude.

Alternatively, we also show the dependence of the SER with the relation $n = T/T_p$. This dependence is shown in Fig. 5
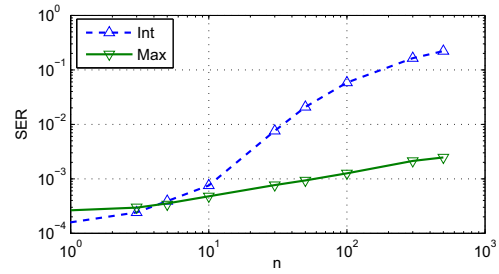
for a fixed distance of 66 mm. As shown, when the time interval T is similar to T_p, we obtain similar performance with both receivers. However, as this relation increases, the proposed receiver outperforms the previous architecture. For nanodevices, where simplicity and consumption must be kept as the main constraints, increasing the time interval means significantly relaxing the design conditions.

D. Regression Model for the SER Estimation

The expressions for the probability density function of the $\max \boldsymbol{X}|s = 0$ and $\max \boldsymbol{X}|s = 1$ functions are composed by the maximum of a large number of chi-square distributions. This fact makes the SER estimation to be difficult to calculate. For this purpose, we derive a regression model for the SER Estimation, based on the observed dependency with the n relation.

Fig. 5 shows that there is a log-log behavior in the SER versus the relation $n = T/T_p$. Moreover, this log-log behavior is approximately constant for any ratio of E/N_0, and even for different noises for "1"s and "0"s, N_{01} and N_{00}. This log-log relation provides a relation between the SER at two different ratios n_1 and n_2 given by:

$$SER_{n_2} = r^{0.45} SER_{n_1} \qquad (15)$$

where $r = T_2/T_1 = n_2/n_1$ is the relation between time intervals.

Then, computing the Engler model [20] to calculate the SER for $n = 1$ with parameter $TW = 3.5$ and by using (15), we can obtain the SER for any distance and n ratio. Fig. 6 shows a comparison between the original model and its regression model. As shown, this regression model matches with the expected value for any of the three distances.

E. Maximum Bitrate

Pulse-based modulation schemes, such as TS-OOK, spread femtosecond-long pulses in time [11]. This time-spread is characterized by a parameter $\beta = T_s/T_p$ and it is usually in the order of $\beta \sim 1000$. For this, in the previous sections, different symbols are considered independent. Although this architecture is proposed mainly to support time-spread pulse-based modulations, this receiver can also support bitrates of up to a few Terabits per second. When the bitrate increases and it gets close to $\beta \sim 1$, the non-idealities of using a low-pass filter to approximate a CTMA plus the pulse overlapping produced by using the second time derivative of a Gaussian pulse affect the system by providing an intersymbol interference (ISI). For this, we have performed a simulation of the Terahertz channel and the receiver architecture considering this overlapping effects between symbols. Fig. 7 shows the achievable
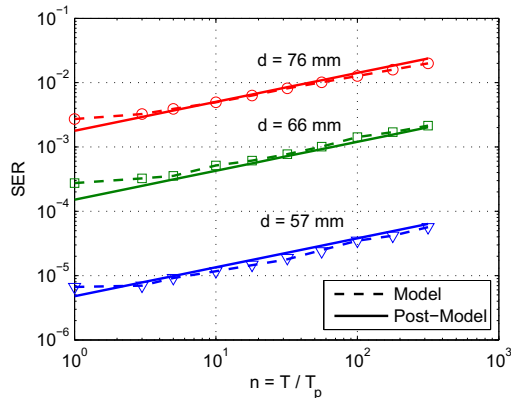
Fig. 6. Comparison of the model with the regression model for the SER estimation. The results are shown for different distances between devices.
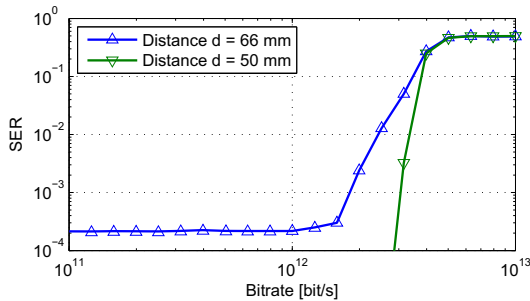

Fig. 7. SER in terms of bitrate.

SER in terms of bitrate for two different distances between nanodevices. As shown, until approximately $R = 2$ Tbit/s the SER is mainly limited by noise, so the SER is kept constant at $SER \approx 2 \cdot 10^{-4}$ for a distance $d = 66$ mm. Then, as soon as the bitrate increases, the receiver is highly affected by the ISI, dropping the SER to $SER = 0.5$ when $R = 5$ Tbit/s. Concerning the distance $d = 50$ mm, the ratio E/N_0 is high enough to neglect the SER when the system is limited by noise. However, as shown in the figure, when the ISI is affecting the receiver, the SER tends to the same values, presenting a $SER = 0.5$ when $R = 5$ Tbit/s.

V. CONCLUSION

Nanonetworks will have a great impact in almost every field of our society, ranging from healthcare to homeland security and environmental protection. For the time being, enabling the communication among nano-devices is still an unsolved challenge. In this paper, we propose a novel receiver architecture for pulse-based electromagnetic nanonetworks in the Terahertz Band. The proposed receiver design is based on a Continuous-Time Moving Average symbol detection scheme, which can be implemented with a single low-pass filter. This symbol detection scheme simplifies the receiver architecture and relaxes the synchronization requirements.

To evaluate the performance of the proposed receiver, we obtain closed-form mathematical expressions for the probability density functions of the received symbols and validate the developed symbol detection model through simulation. Moreover, we compute the symbol error rate for the proposed receiver as a function of different system parameters. Finally, we explore the effects of the inter-symbol interference when the bit-rate is increased up to tens of terabits per second. The results show that this novel symbol detection scheme outperforms existing pulse-radio based detectors when used in the Terahertz Band, by reducing the symbol error rate and increasing the achievable transmission distance for a target SER. Moreover, we show that the proposed scheme can also support bit-rates of up to terabits per second in distances in the order of tens of millimeters using very simple modulations.

VI. ACKNOWLEDGEMENTS

REFERENCES

[1] C. Hierold, A. Jungen, C. Stampfer, and T. Helbling, "Nano electrome-chanical sensors based on carbon nanotubes," *Sensors and Actuators A: Physical*, vol. 136, no. 1, pp. 51 – 61, 2007.

[2] J. M. Dubach, D. I. Harjes, and H. A. Clark, "Fluorescent ion-selective nanosensors for intracellular analysis with improved lifetime and size," *Nano Letters*, vol. 7, no. 6, pp. 1827–1831, 2007.

[3] J. Riu, A. Maroto, and F. X. Rius, "Nanosensors in environmental analysis," *Talanta*, vol. 69, no. 2, pp. 288 – 301, 2006.

[4] I. F. Akyildiz and J. M. Jornet, "Electromagnetic wireless nanosensor networks," *Nano Communication Networks (Elsevier) Journal*, vol. 1, pp. 3–19, March 2010.

[5] P. Avouris, "Carbon nanotube electronics and photonics," *Physics Today*, vol. 62, pp. 34–40, January 2009.

[6] P. Kim, "Toward carbon based electronics," in *IEEE Device Research Conference*, June 2008.

[7] F. Rana, "Graphene terahertz plasmon oscillators," *IEEE Transactions on Nanotechnology*, vol. 7, pp. 91–99, 2008.

[8] J. M. Jornet and I. F. Akyildiz, "Graphene-based nano-antennas for electromagnetic nanocommunications in the terahertz band," in *Proc. of the Fourth European Conference on Antennas and Propagation (EuCAP)*, pp. 1–5, April 2010.

[9] J. M. Jornet and I. F. Akyildiz, "Channel modeling and capacity analysis of electromagnetic wireless nanonetworks in the terahertz band," *to appear in IEEE Transactions on Wireless Communications*, vol. -, pp. –, 2011.

[10] A. Chandrakasan, F. Lee, D. Wentzloff, V. Sze, B. Ginsburg, P. Mercier, D. Daly, and R. Blazquez, "Low-power impulse uwb architectures and circuits," *Proceedings of the IEEE*, vol. 97, pp. 332 –352, February 2009.

[11] J. M. Jornet and I. F. Akyildiz, "Information capacity of pulse-based wireless nanosensor networks," in *Proc. of the 8th Annual IEEE Communications Society Conference on Sensor, Mesh and Ad Hoc Communications and Networks, SECON*, June 2011.

[12] A. Gerosa, S. Solda, A. Bevilacqua, D. Vogrig, and A. Neviani, "An energy-detector for noncoherent impulse-radio uwb receivers," *IEEE Transactions on Circuits and Systems I: Regular Papers*, vol. 56, pp. 1030 –1040, May 2009.

[13] F. Lee and A. Chandrakasan, "A 2.5 nj/bit 0.65 v pulsed uwb receiver in 90 nm cmos," *IEEE Journal of Solid-State Circuits*, vol. 42, pp. 2851 –2859, December 2007.

[14] P. Mercier, M. Bhardwaj, D. Daly, and A. Chandrakasan, "A low-voltage energy-sampling ir-uwb digital baseband employing quadratic correlation," *IEEE Journal of Solid-State Circuits*, vol. 45, pp. 1209 –1219, june 2010.

[15] D. Wentzloff, F. Lee, D. Daly, M. Bhardwaj, P. Mercier, and A. Chandrakasan, "Energy efficient pulsed-uwb cmos circuits and systems," in *Proc. of IEEE International Conference on Ultra-Wideband*, pp. 282 –287, September 2007.

[16] P. Humblet and M. Azizoglu, "On the bit error rate of lightwave systems with optical amplifiers," *Journal of Lightwave Technology*, vol. 9, pp. 1576 –1582, November 1991.

[17] I. Filanovsky and P. Matkhanov, "Synthesis of reactance networks shaping a quasi-rectangular pulse," *IEEE Transactions on Circuits and Systems II: Express Briefs*, vol. 52, pp. 242 – 245, may 2005.

[18] F. T. Roman Sordan and V. Russo, "Logic gates with a single graphene transistor," *Applied Physics Letters*, vol. 94, p. 073305, 2009.

[19] R. Mills and G. Prescott, "A comparison of various radiometer detection models," *IEEE Transactions on Aerospace and Electronic Systems*, vol. 32, pp. 467 –473, jan. 1996.

[20] H. F. Engler and D. H. Howard, "A compendium of analytic models for coherent and non-coherent receivers.," tech. rep., AFWAL-TR-85-1118, Air Force Wright Aeronautical Laboratory,, September 1985.